DELFT UNIVERSITY OF TECHNOLOGY

DEPARTMENT OF AEROSPACE ENGINEERING

Report LR-293

ON THE STRUCTURE OF THE POTENTIAL FLOW FIELD NEAR CONICAL STAGNATION POINTS IN SUPERSONIC FLOW

by

P.G. Bakker
W.J. Bannink
J.W. Reyn

DELFT - THE NETHERLANDS

February 1980

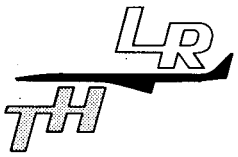

DELFT UNIVERSITY OF TECHNOLOGY

DEPARTMENT OF AEROSPACE ENGINEERING

Report LR-293

ON THE STRUCTURE OF THE POTENTIAL FLOW FIELD NEAR CONICAL STAGNATION POINTS IN SUPERSONIC FLOW

by

P.G. Bakker
W.J. Bannink
J.W. Reyn

DELFT - THE NETHERLANDS

February 1980

SUMMARY

Flow patterns near conical stagnation points in supersonic flow have been investigated on the basis of potential flow. Near the conical stagnation point the non-linear equation for the conical velocity potential reduces to the equation of Laplace. Solution of the equation of Laplace for incompressible plane flow are then used as a guide to generate conical stagnation point solutions. Apart from known types of streamline patterns, such as nodes and saddle points, new types are found. Among them are oblique saddle points, saddle-nodes, topological nodes and topological saddle points.

They may be used to explain certain questions in a number of practical conical flow problems. The oblique saddle point may be used to describe the inviscid flow associated with flow separation and also certain features of the flow over an external corner. The saddle-node, being structurally unstable, may fall apart into a saddle and a node. It may then be used to interprete the lift-off phenomenon of the singularity in the flow around a circular cone at incidence as a bifurcation. Similarly, this may be done for the appearance of a dividing streamline in the same flow at still higher angles of incidence, such that a vortex system is formed at the leeward side of the cone.

CONTENTS

1. INTRODUCTION

In three-dimensional gasdynamics the notion of conical flow has been frequently used, in particular in supersonic flows past conically shaped bodies. In conical flow, the velocity and the conditions defining the state of the gas (pressure, density and temperature) are constant along rays emanating from a common point, the centre of the conical flow field. A conical flow may then be represented on a unit sphere around this centre. The velocity vector may be decomposed into a radial component and a component normal to the radius. From the latter a velocity vector field tangent to the unit sphere may be constructed. Integration of this vector field yields lines on the unit sphere which will be called conical streamlines. Points where the tangential velocity component vanishes will be called conical stagnation points. In conical flows with entropy gradients the entropy remains constant along conical streamlines. Then, if in a conical stagnation point various conical streamlines merge, an entropy singularity or vortical singularity is formed in such a point. This idea was put forward by Ferri (1951) in relation to the supersonic flow past a circular cone at incidence for which he also introduced the concept of the vortical layer near the cone surface. Later investigations of the flow near conical stagnation points show an emphasis of interest in the possible conical streamline patterns, and related pressure distributions near such points. Melnik (1967) constructed some solutions of the exact inviscid conical flow equations in the neighbourhood of a conical stagnation point on a body surface. These solutions involve entropy gradients in the flow. When the streamline pattern was related to the corresponding pressure distribution on the body surface, no unique correspondence was found. Bakker (1977) showed that for these solutions a unique correspondence may be obtained if the pressure distribution normal to the body surface is also taken into account. Both papers indicate that the presence of entropy gradients does not affect the qualitative behaviour of the streamline pattern corresponding to a given pressure distribution. This result is further confirmed

in the special case of the conical stagnation points in the flow past slender circular cones at high incidence, when calculating using slender body theory (Smith 1972), or linearized theory (Bakker & Bannink 1974).

In view of this, in the present report a further study is made of conical stagnation points, using the assumption of potential flow. An advantage of this approach is that the non-linear equations for conical flow reduce to a single second order equation for the conical potential for which solutions are simpler to obtain. Moreover, in a conical stagnation point, this equation becomes the equation of Laplace, which is also satisfied by the velocity potential for an imcompressible plane flow. Stagnation point solutions for incompressible plane flows may then be used as a guide to solutions near conical stagnation points. Also, a comparison of the two types of flows may be made by tracing systematically the influence of the existence of the radial velocity component in the case of conical flow. The analysis in the present report reveals both known streamline patterns as well as new types.

2. POTENTIAL FLOW SOLUTIONS NEAR CONICAL STAGNATION POINTS

Consider an inviscid, non heat conducting, perfect gas with ratio of specific heats $\gamma = \frac{c_p}{c_v}$. If the flow is irrotational, a velocity potential $\Phi = \Phi(x, y, z)$ may be introduced, such that $\nabla\Phi = \underline{q} = (u, v, w)$, where u, v and w are the components of the velocity $\underline{q}$ along the x, y and z axes in a right handed cartesian co-ordinate system, respectively, figure 2.1.

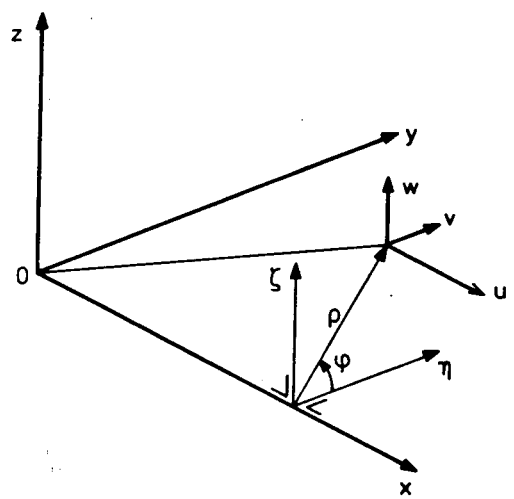

FIG. 2.1 : COORDINATE SYSTEMS AND VELOCITY COMPONENTS.

From the conservation of mass and momentum and the isentropic law, it may be derived that Φ satisfies

$$(a^2 - u^2)\,\Phi_{xx} + (a^2 - v^2)\,\Phi_{yy} + (a^2 - w^2)\,\Phi_{zz} - 2\,uv\,\Phi_{xy}$$

$$- 2\,uw\,\Phi_{xz} - 2\,vw\,\Phi_{yz} = 0, \qquad (2.1)$$

where the speed of sound is related to the velocity by

$$a^2 = \tfrac{1}{2}(\gamma - 1)(q_{max}^2 - u^2 - v^2 - w^2) , \tag{2.2}$$

and q_{max} is the maximum speed corresponding to the total enthalpy, which we assume to be constant throughout the flow field. Equations (2.1) and (2.2) allow velocities to be non-dimensionalized by dividing them by q_{max}; as a result we put $q_{max} = 1$ in (2.2).

We will take the origin (0, 0, 0) in the centre of the conical flow field and the positive x along the ray corresponding to the conical stagnation point. Introducing in (2.1) the conical variables $\eta = y/x$ and $\zeta = z/x$ and the conical potential F defined by

$$\Phi = x\, F(\eta, \zeta) \tag{2.3}$$

yields

$$[a^2(1 + \eta^2) - (v - u\eta)^2]\, F_{\eta\eta} + 2\,[a^2\eta\zeta - (v - u\eta)(w - u\zeta)]\, F_{\eta\zeta} + [a^2(1 + \zeta^2) - (w - u\zeta)^2]\, F_{\zeta\zeta} = 0 , \tag{2.4}$$

where

$$u = F - \eta F_\eta - \zeta F_\zeta , \quad v = F_\eta , \quad w = F_\zeta . \tag{2.5}$$

In the (η, ζ) plane the conical streamlines obey the equation

$$\frac{d\zeta}{d\eta} = \frac{w - u\zeta}{v - u\eta} = \frac{-\zeta F + \eta\zeta F_\eta + (1 + \zeta^2) F_\zeta}{-\eta F + (1 + \eta^2) F_\eta + \eta\zeta F_\zeta} . \tag{2.6}$$

It is sometimes convenient to work with polar co-ordinates $\eta = \rho \cos\varphi$,

$\zeta = \rho \sin \varphi$, $-\infty < \varphi < \infty$, $\rho \geq 0$; then the velocity components become

$$u = F - \rho F_\rho, \quad v = F_\rho \cos \varphi - \frac{1}{\rho} F_\varphi \sin \varphi, \quad w = F_\rho \sin \varphi + \frac{1}{\rho} F_\varphi \cos \varphi, \tag{2.7}$$

and (2.4) can be written as

$$a^2 \left(F_{\rho\rho} + \frac{1}{\rho^2} F_{\varphi\varphi} + \frac{1}{\rho} F_\rho\right) + \left[a^2\rho^2 - \left\{\rho F - (1 + \rho^2) F_\rho\right\}^2\right] F_{\rho\rho}$$

$$+ 2 \left\{F - \left(\rho + \frac{1}{\rho}\right) F_\rho\right\} \left(\frac{1}{\rho} F_{\rho\varphi} - \frac{1}{\rho^2} F_\varphi\right) F_\varphi - \left(\frac{1}{\rho^2} F_{\varphi\varphi} + \frac{1}{\rho} F_\rho\right) \frac{F_\varphi^2}{\rho^2} = 0, \tag{2.8}$$

whereas the conical streamlines obey the equation

$$\frac{d\rho}{d\varphi} = \frac{(1 + \rho^2)\, \rho^2 F_\rho - \rho^3 F}{F_\varphi} \tag{2.9}$$

The direction of flow on a conical streamline may be obtained from

$$x \frac{d\eta}{dt} = v - u\eta, \quad x \frac{d\zeta}{dt} = w - u\zeta\ , \tag{2.10}$$

or

$$x \frac{d\rho}{dt} = (1 + \rho^2) F_\rho - \rho F\ , \quad x \frac{d\varphi}{dt} = \frac{1}{\rho^2} F_\varphi\ , \tag{2.11}$$

where t indicates time.

With the chosen co-ordinate system, the conical stagnation point is located in $\eta = \zeta = 0$ and since $v = w = o$ there, (2.4) yields

$$F_{\eta\eta}(0, 0) + F_{\zeta\zeta}(0, 0) = 0\ . \tag{2.12}$$

If the velocity components are assumed to be continuous in a neighbourhood of the origin, (2.12) shows that (2.4) in this neighbourhood is approximately the equation of Laplace, which is also satisfied by the velocity potential in incompressible plane flow. In polar co-ordinates, stagnation point solutions for plane incompressible flow are given by

$$\Phi = a_n \rho^n \cos(n\varphi + \psi_n) , \quad n > 1 , \tag{2.13}$$

where a_n, ψ_n are constants. They represent flows in corners with opening angles $\alpha = \frac{\pi}{n}$; thus $0 < \alpha < \pi$. The streamline pattern is well known.

In analogy, we seek conical stagnation point solutions of (2.8) in the form of the series expansion

$$F = F_0 + \rho^n F_n(\varphi) + \rho^m F_m(\varphi) + o(\rho^m) , \quad 1 < n < m , \tag{2.14}$$

where F_0 is a constant, which is irrelevant in plane flow. In conical flow, however, F_0, which equals the non-dimensionalized radial velocity component u_o in the conical stagnation point (equation (2.5)), enters in the conical streamline pattern (equation (2.6)). As a result, depending on its magnitude, it may have a significant effect on this streamline pattern. In this reportwe only consider supersonic conical stagnation points, so that $a_0 < |F_0| < 1$, where a_0 is the speed of sound in the conical stagnation point.
It may be useful to remark, that positive and negative values of F_0 are allowed in the present analysis; in most practical flow situations, however, $F_0 > 0$.

If (2.14) is substituted into (2.8) and the result ordered with respect to powers in ρ, the coefficient of the lowest order term appears to be

$$F_n'' + n^2 F_n = 0 \tag{2.15}$$

with the solutions

$$F_n(\varphi) = a_n \cos(n\varphi + \psi_n) \quad , n > 1 \tag{2.16}$$

where a_n and ψ_n are arbitrary constants. Thus this term exactly equals the stagnation point solution for plane flow (see (2.13)). We may use the freedom, still existing in the choice of the co-ordinate system, to rotate the co-ordinate system around the x-axis such that $\psi_n = 0$ in (2.16).

When the next higher order terms are written out, several cases for n and m have to be distinguished. After equating the coefficient of the next lowest order term to zero there follows

$\underline{1 < n < 2}$

$$F_m'' + m^2 F_m = 0 \quad , n < m < 3n-2 , \tag{2.17}$$

$$F_m'' + m^2 F_m = n^3(n-1)\, a_0^{-2} F_n^3 + n(n-1)\, a_0^{-2} F_n (F_n')^2 , \quad m = 3n-2, \tag{2.18}$$

$$n(n-1) F_n \left[n^2 F_n^2 + (F_n')^2 \right] = 0 \quad , m > 3n-2, \tag{2.19}$$

with the solutions

$$F_m(\varphi) = b_m \cos(m\varphi + \psi_m) \quad , n < m < 3n-2, \tag{2.20}$$

$$F_m(\varphi) = b_m \cos(m\varphi + \psi_m) + \frac{n^2 a_n^3}{4a_0^2(2n-1)} \cos n\varphi \quad , m = 3n-2, \tag{2.21}$$

whereas (2.19) yields $F_n(\varphi) \equiv 0$, which means that $m > 3n-2$ cannot occur. In (2.20), (2.21) b_m and ψ_m are arbitrary constants.

$\underline{n = 2}$

$$F_m'' + m^2 F_m = 0 \quad , 2 < m < 4, \tag{2.22}$$

$$F_m'' + m^2 F_m = -2\left[1 - a_0^{-2}(F_0 - 2F_2)^2\right] F_2 - 2a_0^{-2}(F_0 - F_2)(F_2')^2,$$

$$m = 4 , \qquad (2.23)$$

$$F_2\left[a_0^2 - (F_0 - 2F_2)^2\right] + (F_0 - F_2)(F_2')^2 = 0, \; m > 4 , \qquad (2.24)$$

with the solutions

$$F_m(\varphi) = b_m \cos(m\varphi + \psi_m) \quad , 2 < m < 4 , \qquad (2.25)$$

$$F_m(\varphi) = b_m \cos(m\varphi + \psi_m) - \frac{a_2^2 F_0}{2a_0^2} - \frac{a_2(a_0^2 - F_0^2 - 4a_2^2)}{6a_0^2}\cos 2\varphi ,$$

$$, m = 4 , \qquad (2.26)$$

whereas (2.24) yields $F_2(\varphi) \equiv 0$, which indicates that $m > 4$ cannot occur. In (2.25), (2.26) b_m and ψ_m are arbitrary constants.

$n > 2$

$$F_m'' + m^2 F_m = 0 \quad , n < m < n+2, \qquad (2.27)$$

$$F_m'' + m^2 F_m = -\left(1 - \frac{F_0^2}{a_0^2}\right) n(n-1) F_n \quad , m = n+2, \qquad (2.28)$$

$$n(n-1)(a_0^2 - F_0^2) F_n = 0 \quad , m > n+2, \qquad (2.29)$$

with the solutions

$$F_m(\varphi) = b_m \cos(m\varphi + \psi_m) \quad , n < m < n+2, \qquad (2.30)$$

$$F_m(\varphi) = b_m \cos(m\varphi + \psi_m) - \frac{n(n-1)}{m^2 - n^2} a_n \left(1 - \frac{F_0^2}{a_0^2}\right) \cos n\varphi,$$

$$, m = n+2, \qquad (2.31)$$

whereas (2.29) yields $F_n(\varphi) \equiv 0$, which means that $m > n+2$ cannot occur. In (2.30), (2.31) b_m and ψ_m are arbitrary constants. Figure 2.2 shows the values of n and m for which it is possible to determine the functions $F_n(\varphi)$ and $F_m(\varphi)$ in the expansion given by (2.14).

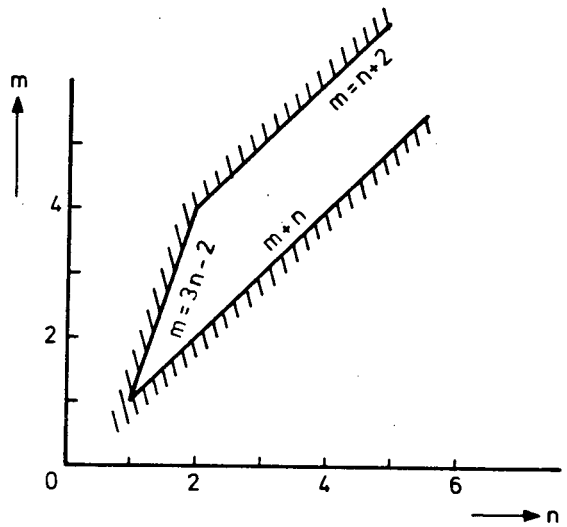

FIG. 2.2 : VALUES OF n AND m FOR WHICH $F_n(\varphi)$ AND $F_m(\varphi)$ EXIST.

With the aid of the listed solutions for the conical velocity potential and (2.6) or (2.9) the conical streamline pattern near the conical stagnation point may be determined. The pressure distribution follows from the relation

$$\left(\frac{p}{p_0}\right)^{\frac{\gamma-1}{\gamma}} = \left(\frac{a}{a_0}\right)^2 = \frac{1 - (u^2 + v^2 + w^2)}{1 - u_0^2} , \qquad (2.32)$$

where the zero subscript indicates conditions in the conical stagnation point.

3. FIRST ORDER SOLUTIONS NEAR CONICAL STAGNATION POINTS (FIRST ORDER SINGULARITIES)

3.1. The equation of the conical streamlines

The conical streamline pattern near a conical stagnation point is obtained by substitution of the solutions for $F_n(\varphi)$ and $F_m(\varphi)$ into the differential equations (2.6) or (2.9).
Then, after expanding the conical potential (2.14) and its derivatives in powers of ρ, we obtain

$$\frac{d\rho}{d\varphi} = \frac{-\rho^3 F_0 + n\,\rho^{n+1} F_n(\varphi) + (n-1)\,\rho^{n+3} F_n(\varphi) + m\,\rho^{m+1} F_m(\varphi) + o(\rho^{m+1})}{\rho^n F_n'(\varphi) + \rho^m F_m'(\varphi) + o(\rho^m)} \tag{3.1}$$

where $m > n$.
The correct order of terms in the numerater of (3.1) depends upon the relative value of $m + 1$ with respect to $n + 3$, a knowledge which is not present a priori.
Therefore in the following, n and m are assumed to have known values.
Now, if a parameter τ is introduced, the qualitative behaviour of the integral curves near $\rho = 0$ may be found by the investigation of (3.1) as a system in the (φ,ρ) plane, then

$$\frac{d\rho}{d\tau} = -\rho^{3-n} F_0 + n\,\rho\, F_n(\varphi) + (n-1)\,\rho^3 F_n(\varphi) + m\,\rho^{m-n+1} F_m(\varphi) + o(\rho^{m-n+1})$$

$$\frac{d\varphi}{d\tau} = F_n'(\varphi) + \rho^{m-n} F_m'(\varphi) + o(\rho^{m-n}) \tag{3.2}$$

The singular points of this system at $\rho = 0$ are in $\varphi = \varphi_s$, where φ_s may be determined if the functions $F_n(\varphi)$ and $F_m(\varphi)$ are specified.
The conical streamlines near $\rho = 0$ are governed by the solution of the

system (3.2) in the vicinity of its singular points; this solution may be obtained by local linearization. It may be shown (Andronov et al. 1973 p. 126) that for non vanishing real parts of the eigenvalues of the coefficient matrix of the linearized system the higher order terms do not modify the local character of the integral curves. These particular solutions are called first order solutions and consequently the corresponding conical stagnation points are defined as first order singularities.
In the cases where one of the real parts of the eigenvalues is zero, higher order terms have to be retained in the analysis; they will be discussed in paragraph 4.

3.2. Oblique saddle points ($1 < n < 2$)

Substitution of (2.16), (2.20), (2.21) into (2.14), and (2.14) into (2.9) leads to the equation for the conical streamlines

$$\frac{d\rho}{d\varphi} = \frac{n a_n \rho^{n+1} \cos n\varphi - F_0 \rho^3 + O(\rho^{m+1})}{-n a_n \rho^n \sin n\varphi + O(\rho^m)} . \tag{3.3}$$

Introducing a parameter τ along the streamlines, we investigate (3.3) as a system in the (φ, ρ) plane. Then

$$\begin{aligned} \frac{d\varphi}{d\tau} &= - \sin n\varphi + O(\rho^{m-n}) , \\ \frac{d\rho}{d\tau} &= \rho \cos n\varphi - \frac{F_0}{n a_n} \rho^{3-n} + O(\rho^{m-n+1}) . \end{aligned} \tag{3.4}$$

The singular points of this system for $\rho = 0$ are in $\varphi = \frac{k\pi}{n}$ ($k = 0, \pm 1, \pm 2, \ldots$), which appear to be saddle points for the locally linearized system. It may be shown that the real parts of the eigenvalues of this system are non zero, so the higher order terms do not modify the saddle point character of these singular points. Retaining only the lowest order terms in (3.4) yields, upon integration, the approximate shape

of the conical streamlines

$$\rho^n \sin n\varphi = C \ , \tag{3.5}$$

where $C \geq 0$ is a constant. It is well known that (3.5) also represents the streamlines in an incompressible stagnation point flow. Equation (3.5) represents the streamline pattern for a flow in a corner with an including angle $\alpha = \frac{\pi}{n}$, thus $\frac{\pi}{2} < \alpha < \pi$ for $1 < n < 2$. Obviously, it is not possible to fill out a full neighbourhood ($0 \leq \varphi < 2\pi$) of the conical stagnation point with corner flows, such that the velocity is continuous. The conical stagnation point can therefore only occur on a body surface, with one or more streamlines coinciding with the body surface.

From (2.7) and (2.14) the velocity components may be obtained as

$$\begin{aligned} u &= F_0 - (n-1)\, a_n\, \rho^n \cos n\varphi + O(\rho^m), \\ v &= n a_n\, \rho^{n-1} \cos (n-1)\, \varphi + O(\rho^{m-1}) \ , \\ w &= -n a_n\, \rho^{n-1} \sin (n-1)\, \varphi + O(\rho^{m-1}). \end{aligned} \tag{3.6}$$

The pressure distribution then follows from (2.32) and (3.6)

$$\left(\frac{p}{p_0}\right)^{\frac{\gamma-1}{\gamma}} = 1 - \frac{n^2 a_n^2}{1 - F_0^2}\, \rho^{2n-2} + O(\rho^{n+m-2}) \ . \tag{3.7}$$

The pressure attains a maximum in the conical stagnation point, and the isobars are to a first approximation concentric circles around the

origin, as shown in figure 3.1 by the dashed lines. Also shown in figure 3.1 is the streamline pattern in a corner $k\frac{\pi}{n} < \varphi < (k+1)\frac{\pi}{n}$. The direction of flow on these streamlines corresponds to $a_n \cos k\pi < 0$; if $a_n \cos k\pi > 0$ the flow direction should be reversed. This follows from (2.11), (2.14), (2.16), (2.20), (2.21) which yield

$$x \frac{d\rho}{dt} = n a_n \rho^{n-1} \cos n\varphi - F_0 \rho + O(\rho^{m-1}) \quad . \tag{3.8}$$

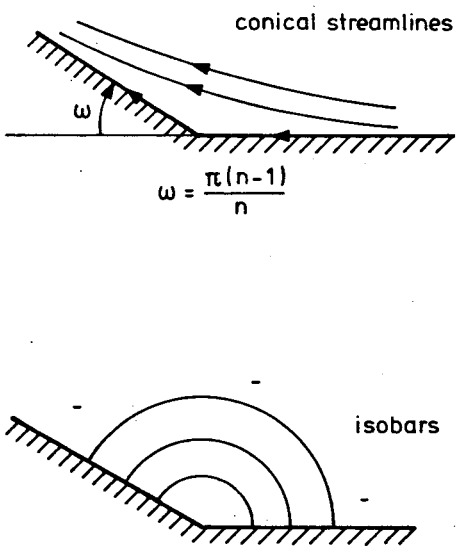

FIG. 3.1 : OBLIQUE SADDLE (1<n<2)

Oblique saddle points as stagnation points occur in the corner point of the supersonic flow past an external axial corner. This type of flow was treated numerically by Kutler & Shankar (1976). It was also analyzed by Salas & Daywitt (1978) on the basis of the assumption that the velocity and pressure gradient at the corner point are regular.

Equations (3.6), (3.7) show, however, that saddle point solutions are possible with singular gradients if the including angle is between $\frac{2}{3}\pi$ and π rad. As a result, the Kutler-Shankar model for symmetric and asymmetric flow past the corner is not necessarily based on a wrong boundary condition at the corner, as stated by Salas & Daywitt (1978). Moreover, the conclusions given by Salas & Daywitt (1978) for the flow structure near the symmetric corner are hindered by the fact that in their analysis the determinant of the Hessian matrix for the pressure is incorrect, it should be divided by a $\sin^2\theta$, which vanishes at the conical stagnation point.

3.3. Nodes and saddle points (n = 2)

Substitution of (2.16), (2.25), (2.26) into (2.14) and (2.14) into (2.6) leads to the equation for the conical streamlines

$$\frac{d\zeta}{d\eta} = \frac{-(2a_2+F_0)\zeta+(mF_m\sin\varphi+F_m'\cos\varphi)\rho^{m-1}+a_2\rho^3\sin\varphi\cos 2\varphi+O(\rho^{m+1})}{(2a_2-F_0)\eta+(mF_m\cos\varphi-F_m'\sin\varphi)\rho^{m-1}+a_2\rho^3\cos\varphi\cos 2\varphi+O(\rho^{m+1})}, \quad (3.9)$$

where $\rho = (\eta^2 + \zeta^2)^{\frac{1}{2}}$, $\varphi = \tan^{-1}(\eta^{-1}\zeta)$. When (3.9) is written as a system and only the linear terms are retained, there follows

$$\begin{aligned} \frac{d\eta}{d\tau} &= (-1 + 2\lambda)\,\eta\,, \\ \frac{d\zeta}{d\tau} &= (-1 - 2\lambda)\,\eta\,, \end{aligned} \quad (3.10)$$

where $\lambda = a_2 F_0^{-1}$, λ may be identified with the value of the derivatives $\frac{1}{u_0}\frac{dv}{d\eta}$ or $\frac{1}{u_0}\frac{dw}{d\zeta}$ in the conical stagnation point.

The eigenvalue of the coefficient matrix are

$$\mu_{1,2} = -1 \pm 2\lambda. \tag{3.11}$$

From (3.11) we may conclude that for $|\lambda| = \frac{1}{2}$ the eigenvalues are zero and consequently higher order singularities occur.

For $|\lambda| \neq \frac{1}{2}$ none of the eigenvalues $\mu_{1,2}$ is equal to zero and the solutions of (3.10) may be expected to give an approximation of the streamline pattern near the conical stagnation point. Equations (2.25), (2.26), however, show that for $2 < m < 3$, $3 < m < 4$ the function $F_m(\varphi)$ is not periodic with period 2π, therefore it is not possible to fill out a full neighbourhood of the stagnation point, such that the velocity is continuous. For $2 < m < 3$ and $3 < m < 4$ parts of the solutions between streamlines may be used to construct flows near conical stagnation points on a body surface. If $m = 3$ or $m = 4$ the behaviour of $F_m(\varphi)$ does not hinder the conical stagnation point to appear in the flow field away from a body surface. If this remains to be true when all higher order terms are added, the point can be realized in the flow, and the character of the singularity in the streamline pattern is determined by (3.10) (Coddington & Levinson 1955). The singularity of (3.10) is a starlike node for $\lambda = 0$, and a node with two perpendicular approach directions for the streamlines for $0 < |\lambda| < \frac{1}{2}$, whereas it is a saddle point with orthogonal separatrices for $|\lambda| > \frac{1}{2}$. It may be observed that a large value of $|\lambda|$ corresponds to a value of F_0 ($F_0 = u_0$ = radial velocity in the conical stagnation point), being small compared to a_2, which is the stagnation point solution in incompressible flow. The flow pattern then resembles that which is also observed in incompressible plane flow. If $|\lambda|$ is decreased, the radial velocity becomes more dominant and for $|\lambda| < \frac{1}{2}$ the streamline pattern forms a node, which is not observed in incompressible plane flow.

Sketches of the conical streamline pattern are given in figure 3.2 for $F_0 > 0$; for $F_0 < 0$ the direction of the streamlines is reversed.

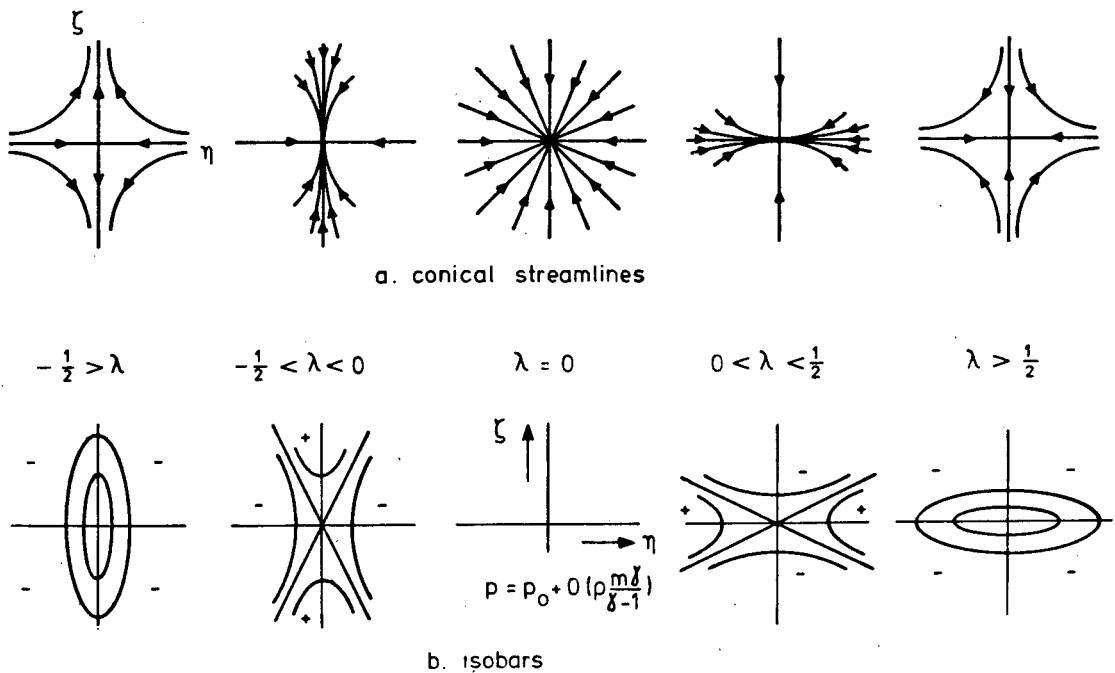

FIG. 3.2 : NODES AND SADDLES ($n = 2$, $m = 3$ OR 4, $|\lambda| \neq 1/2$)

The direction may be obtained from

$$x \frac{d\eta}{dt} = 2F_0(\lambda - \tfrac{1}{2})\,\eta + O((\eta^2 + \zeta^2)^{\frac{1}{2}}) ,$$
$$x \frac{d\zeta}{dt} = -2F_0(\lambda + \tfrac{1}{2})\,\zeta + O((\eta^2 + \zeta^2)^{\frac{1}{2}}), \qquad (3.12)$$

which may be derived from (2.10), (2.5), (2.14).

From (2.7), (2.14) the velocity components may be obtained to be

$$u = F_0 - a_2 \rho^2 \cos 2\varphi - (m-1) \rho^m F_m + o(\rho^m) ,$$

$$v = 2a_2 \rho \cos \varphi + (mF_m \cos \varphi - F_m' \sin \varphi) \rho^{m-1} + o(\rho^{m-1}) , \qquad (3.13)$$

$$w = -2a_2 \rho \sin \varphi + (mF_m \sin \varphi + F_m' \cos \varphi) \rho^{m-1} + o(\rho^{m-1}).$$

The pressure distribution then follows from (2.32), (3.13)

$$\left(\frac{p}{p_0}\right)^{\frac{\gamma-1}{\gamma}} = 1 - \frac{4\lambda F_0^2}{1 - F_0^2} (\lambda - \tfrac{1}{2}) \eta^2 + (\lambda + \tfrac{1}{2}) \zeta^2 + o(\rho^m) . \qquad (3.14)$$

A sketch of the isobars is given in figure 3.2.
If $|\lambda| > \frac{1}{2}$, thus when a saddle point singularity for the streamlines occurs, the pressure attains a maximum in the conical stagnation point and the isobars are to a first approximation concentric ellipses around the origin. Again the similarity with the incompressible case (and the case $1 < n < 2$) is obvious. If $0 < |\lambda| < \frac{1}{2}$ - the streamlines then have a nodal singularity - the isobars are to a first approximation concentric hyperbolas with asymptotes given by

$$\zeta = \pm \sqrt{\frac{\frac{1}{2} - \lambda}{\frac{1}{2} + \lambda}} \eta . \qquad (3.15)$$

In the regions within the acute angle between the asymptotes the pressure is higher than in the conical stagnation point, whereas in the other regions the pressure is lower. Comparison of the isobars with the streamline pattern shows that in the direction along which an infinite number of streamlines approach, the pressure has a minimum, whereas in the direction along which only one streamline approaches, the pressure has a maximum. For $\lambda = 0$ the pressure does not change to the order $\frac{m\gamma}{\gamma-1}$ in

the distance from the conical stagnation point; this case actually corresponds to $n > 2$ and will be further discussed later. The singularities in the streamline patterns, discussed in this section belong to the class of structurally stable singularities and consist of nodes and saddle points. They are structurally stable in the sense that small changes in the flow solutions, for instance, caused by small changes in a parameter, such as the angle of incidence of a conical body, leave the character of the singularity invariant. These nodes and saddle points are mentioned in the conical flow literature at various places; in fact they already appear in the first paper on this subject (Ferri 1951). Particular attention has been given to the conical stagnation point(s) in the leeward symmetry plane of the supersonic flow past a circular cone at incidence. The change of the nodal character in this point on the body surface with angle of incidence up to moderate angles of incidence is discussed in several references, i.e. Melnik (1967), Smith (1972), Bakker & Bannink (1974) and Bakker (1977).

3.4. Starlike nodes $n > 2$

Substitution of (2.16), (2.30), (2.31) into (2.14), and (2.14) into (2.9) leads to the equation for the conical streamlines

$$\frac{d\rho}{d\varphi} = \frac{-F_0\,\rho^3 + n a_n\,\rho^{n+1}\cos n\varphi + O(\rho^{m+1})}{-n a_n\,\rho^n \sin n\varphi + O(\rho^m)} \tag{3.16}$$

which, in fact, is equal to (3.3) for the case $1 < n < 2$. Comparison of (3.3) and (3.16), however, shows the more dominating influence of the (radial) velocity component F_0 in the conical stagnation point in the case $n > 2$. Introducing the parameter τ along the streamlines we investigate (3.16) as a system in the (φ, σ) plane, where $\sigma = \rho^{n-2}$ $(\sigma \geq 0)$, instead of ρ the variable σ is used in order to arrive at a system which is analytic in its leading terms.

Then

$$\frac{d\varphi}{d\tau} = -na_n \sin n\varphi + O\left(\sigma^{\frac{m-n}{n-2}}\right),$$
$$\frac{d\sigma}{d\tau} = -(n-2)\, F_0 + n(n-2)\, a_n\, \sigma \cos n\varphi + O\left(\sigma^{1+\frac{m-n}{n-2}}\right). \qquad (3.17)$$

The line $\sigma \equiv 0$ thus contains only regular points of (3.17), as a result of which through any point of this line there exists a unique integral curve of (3.17), figure 3.3.

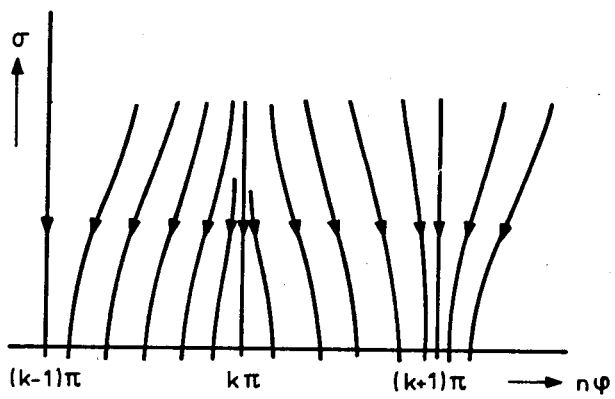

FIG. 3.3 : INTEGRAL CURVES IN THE (φ, σ) PLANE $(n > 2)$

Correspondingly, in the (η, ζ) plane, there is one and only one streamline, approaching the origin in any direction within a sector near the conical stagnation point. It is natural from (3.16) to consider sectors with an opening angle, which is a multiple of $\alpha = \frac{\pi}{n}$ rad, thus $0 < \alpha < \frac{\pi}{2}$ for $n > 2$.

If n is not an integer, it is not possible to fill out a full neighbourhood of the conical stagnation point with these sectors, such that the velocity is continuous. Such flowsmay therefore only be obtained near

a conical stagnation point on a body surface. Conical stagnation points away from a body surface can only occur if n is an integer. Sketches of the streamline patterns are given in figure 3.4 ($F_0 > 0$).

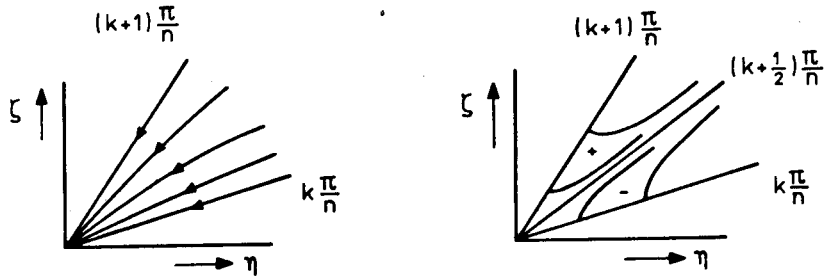

a. conical streamlines b. isobars

FIG. 3.4: STARLIKE NODE (n>2)

Substituting (2.16), (2.30) into (2.14) and using (2.7), we obtain for the pressure distribution, from (2.32)

$$\left(\frac{p}{p_0}\right)^{\frac{\gamma}{\gamma-1}} = 1 + \frac{2F_0(n-1)\,a_n}{1-F_0^2}\,\rho^n \cos n\varphi + O(\rho^m) + O(\rho^{2n-2}) \quad . \qquad (3.18)$$

The isobar pattern resulting from (3.18) shows a saddle character and is also sketched in figure 3.4.

Comparison with the incompressible plane stagnation point solution, which is a saddle point type flow in a corner with opening angle less than $\pi/2$ rad, shows that the dominance of F_0 makes such a flow impossible in conical stagnation point flows. It should be stressed, however, that this result is obtained under the assumption of potential flow and need not be valid in flows with entropy gradients.

In fact, preliminary calculations show that such corner flows with entropy gradients exist. In conjunction with oblique saddle point flows, they may probably be used to describe the structure of inviscid flow near flow separation from a body surface such as the flow past a circular cone at high angles of incidence. This structure was investigated by Fletcher(1975), Bannink & Nebbeling(1978), McRae & Hussaini (1978), Nebbeling & Bannink(1978).

An example of the singularity for $n > 2$ is the conical stagnation point in a parallel flow (then $a_n = 0$).

4. HIGHER ORDER SOLUTIONS NEAR CONICAL STAGNATION POINTS (HIGHER ORDER SINGULARITIES)

In the previous paragraph there was pointed out that higher order singularities occur only in the case $n = 2$, because then, for $|\lambda| = \frac{1}{2}$, one of the eigenvalues $\mu_{1,2}$ given by (3.11) is equal to zero and the non-linear terms in (3.9) cannot be neglected when considering the streamline pattern. From (3.9) it is clear that we should distinguish two cases: $2 < m < 4$ and $m = 4$.

4.1. Saddle-nodes, topological saddle points, topological nodes ($2 < m < 4$)

For $\lambda = \pm \frac{1}{2}$ equations (2.14), (2.16), (2.25) show that the conical potential may be written as

$$F = F_0 \left[1 \pm \tfrac{1}{2}\rho^2 \cos 2\varphi + \frac{2\mu}{m} \rho^m \cos (m\varphi + \psi_m) + o(\rho^m)\right] , \qquad (4.1)$$

where $\mu = \dfrac{mb_m}{2F_0}$. We restrict ourselves to $\lambda = -\frac{1}{2}$; the case $\lambda = \frac{1}{2}$ may be obtained by taking the minus sign in (4.1) and replacing φ and ψ_m by $\varphi + \frac{\pi}{2}$ and $\psi_m - m\frac{\pi}{2}$, respectively. Substition of (4.1) into (2.9) leads to the equation for the conical streamlines

$$\frac{d\rho}{d\varphi} = \frac{-\rho \cos^2 \varphi + \mu \rho^{m-1} \cos (m\varphi + \psi_m) + O(\rho^3)}{\sin \varphi \cos \varphi - \mu \rho^{m-2} \sin (m\varphi + \psi_m) + o(\rho^{m-2})} . \qquad (4.2)$$

Using the parameter τ along the streamlines, we investigate (4.2) as a system in the (φ, σ) plane, where $\sigma = \rho^{m-2}$ $(\sigma \geq 0)$. Then

$$\begin{aligned} \frac{d\varphi}{d\tau} &= \sin \varphi \cos \varphi - \mu \sigma \sin (m\varphi + \psi_m) + o(\sigma) , \\ \frac{d\sigma}{d\tau} &= -(m-2) \sigma \cos^2 \varphi + (m-2) \mu \sigma^2 \cos (m\varphi + \psi_m) + O\left(\sigma^{\frac{m}{m-2}}\right) \end{aligned} \qquad (4.3)$$

The singular points of this system for $\sigma = 0$ are in $\varphi = \varphi_\ell = \frac{1}{2}\ell\pi$ ($\ell = 0, \pm 1, \pm 2, \ldots$). Expanding with respect to $\varphi - \varphi_\ell$ and retaining only terms up till second order yields from (4.3)

$$\frac{d\varphi}{d\tau} = ab + (-a^2 + b^2)(\varphi - \varphi_\ell) - A_\ell\,\sigma - 2ab(\varphi - \varphi_\ell)^2 - mB_\ell(\varphi - \varphi_\ell)\sigma ,$$

$$\frac{d\sigma}{d\tau} = -(m-2)\,b^2\,\sigma + 2(m-2)\,ab(\varphi - \varphi_\ell)\,\sigma + (m-2)\,B_\ell\,\sigma^2 , \qquad (4.4)$$

where $a = \sin\varphi_\ell$, $b = \cos\varphi_\ell$, $A_\ell = \mu \sin(m\varphi_\ell + \psi_m)$, $B_\ell = \mu\cos(m\varphi_\ell + \psi_m)$. There are two cases: ℓ even, $a = 0$, $b^2 = 1$ and ℓ odd, $a^2 = 1$, $b = 0$. If (4.4) is linearized the eigenvalues of the coefficient matrix are given by

$$\mu_1 = -a^2 + b^2, \quad \mu_2 = -(m-2)\,b^2 . \qquad (4.5)$$

If ℓ is even, $\varphi = \varphi_\ell$, $\sigma = 0$ is a saddle point, also for the non-linear system (4.4). Sketches of the streamline pattern in the (φ, σ) plane are given in figure 4.1. The separatrices make the angle ω with the $\varphi - \varphi_\ell$ axis, where $\omega = 0$ or $\tan^{-1}(m-1)\,A_\ell^{-1}$. The flow direction corresponds to $F_0 > 0$. It should be noted that only $\sigma \geq 0$ is of interest for the present investigation.

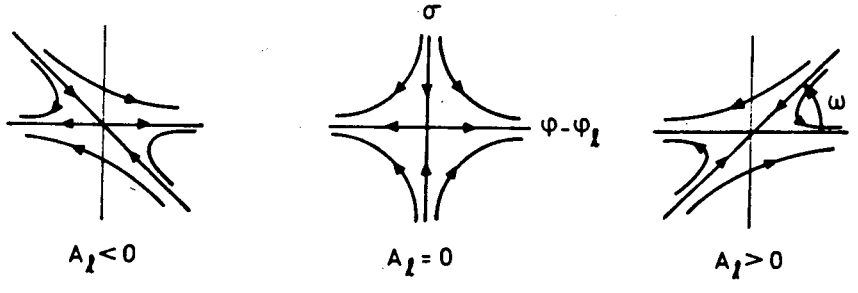

FIG. 4.1 : PATTERN OF CONICAL STREAMLINES IN (φ, σ) PLANE NEAR $\varphi = \varphi_\ell = \frac{\pi}{2}\ell, \ell = 0, \pm 2, \pm 4, \ldots\ldots$ $(n = 2, 2 < m < 4, \lambda = -\frac{1}{2})$

If ℓ is odd, (4.5) yields $\mu_1 = -1$, $\mu_2 = 0$ and higher order terms cannot be neglected. Expanding (4.3) and retaining only terms till third order yields

$$\frac{d\varphi}{d\tau} = -(\varphi - \varphi_\ell) - A_\ell\,\sigma - mB_\ell(\varphi - \varphi_\ell)\,\sigma\,,$$

$$\frac{d\sigma}{d\tau} = (m-2)\,B_\ell\,\sigma^2 - (m-2)(\varphi - \varphi_\ell)^2\,\sigma - m(m-2)\,A_\ell(\varphi - \varphi_\ell)\,\sigma^2\,. \tag{4.6}$$

For $\varphi = \varphi_\ell$, $\sigma = 0$ system (4.6) has a multiple equilibrium point with $\mu_1 + \mu_2 = -1 \neq 0$. This permits us to follow the line of analysis given by Andronov et al. (1973) and summirized in the Appendix.

Take first $A_\ell \neq 0$. Then, by the change of variables $\varphi^* = -(\varphi - \varphi_\ell) - A_\ell\,\sigma$, $\sigma^* = -A_\ell\,\sigma$ and $\tau^* = -\tau$, we obtain from (4.6)

$$\frac{d\varphi^*}{d\tau^*} = \varphi^* - m\,\frac{B_\ell}{A_\ell}\,\varphi^*\,\sigma^* + 2(m-1)\,\frac{B_\ell}{A_\ell}\,\sigma^{*2} + O((\varphi^{*2} + \sigma^{*2})^{3/2}),$$

$$\frac{d\sigma^*}{d\tau^*} = (m-2)\,\frac{B_\ell}{A_\ell}\,\sigma^{*2} + O((\varphi^{*2} + \sigma^{*2})^{3/2})\,, \tag{4.7}$$

from which follows that $\frac{d\varphi^*}{d\tau^*} = 0$ on the curve

$$\varphi^* = f(\sigma^*) = -2(m-1)\,\frac{B_\ell}{A_\ell}\,\sigma^{*2} + O(\sigma^{*3})\,, \tag{4.8}$$

and that on this curve

$$\frac{d\sigma^*}{d\tau^*} = \Delta_k \sigma^{*k} + O(\sigma^{*k+1}) = (m-2)\frac{B_\ell}{A_\ell}\sigma^{*2} - (m-1)(m-2)\sigma^{*3} + O(\sigma^{*4}) \tag{4.9}$$

For $B_\ell \neq 0$, there follows $k = 2$, and, according to Theorem I in the Appendix the equilibrium point is a saddle-node. It has one parabolic (nodal type) sector and two hyperbolic (saddle point type) sectors. If $\frac{B_\ell}{A_\ell} < 0$ the hyperbolic sectors contain a segment of the positive σ^* axis and if $\frac{B_\ell}{A_\ell} > 0$ they contain a segment of the negative σ^* axis. For $B_\ell = 0$, there follows $k = 3$, $\Delta_k < 0$ and the equilibrium point is a topological saddle point, whose separatrices are directed along the φ^*, σ^* axes.

For $A_\ell \neq 0$ the streamline pattern may now be sketched in the (φ, σ) plane, as is done in figure 4.2a. The separatrices include an angle ω with the $\varphi - \varphi_\ell$ axis, where $\omega = 0$ or $\tan^{-1} A_\ell^{-1}$, the latter value also indicating the approach direction for streamlines in a nodal part of the singularity. The flow directions in figure 4.2a correspond to $F_0 > 0$. It should be noted that only $\sigma \geq 0$ is of interest for the present investigation.

Now take $A_\ell = 0$. Since $A_\ell^2 + B_\ell^2 = \mu^2$, and $\mu = 0$ cannot occur in the proposed expansion given in (4.1), $A_\ell = 0$ implies $B_\ell \neq 0$. Then, by the change of variables $\varphi^* = \varphi - \varphi_\ell$, $\sigma^* = \sigma$ and $\tau^* = -\tau$, (4.6) becomes

$$\begin{aligned} \frac{d\varphi^*}{d\tau^*} &= \varphi^* + mB_\ell \varphi^* \sigma^* , \\ \frac{d\sigma^*}{d\tau^*} &= -(m-2) B_\ell \sigma^{*2} + O((\varphi^{*2} + \sigma^{*2})^{3/2}) , \end{aligned} \tag{4.10}$$

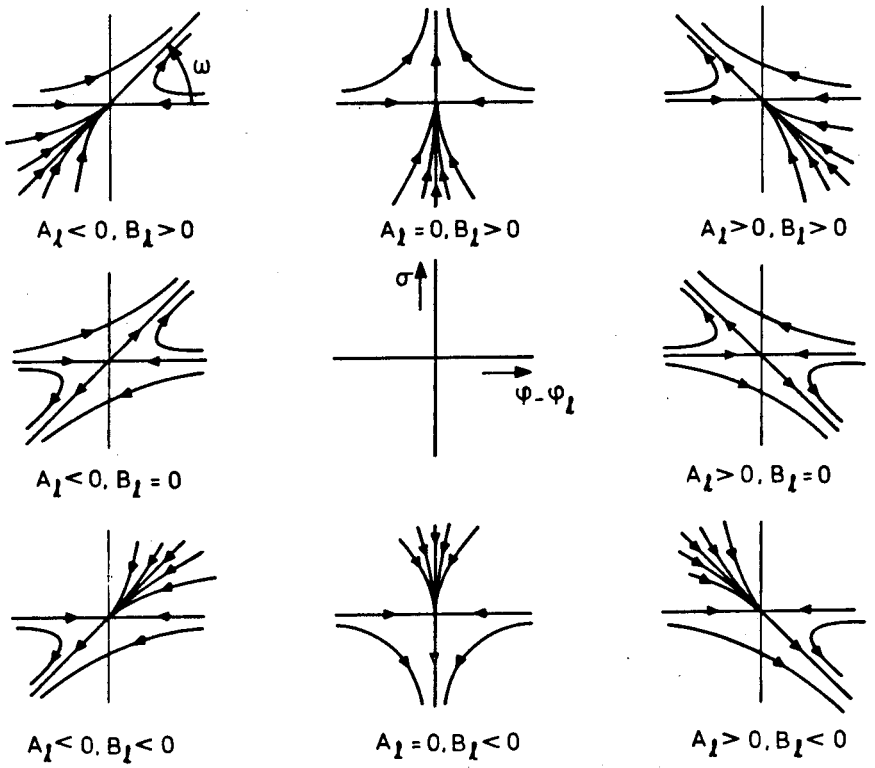

a. conical streamlines

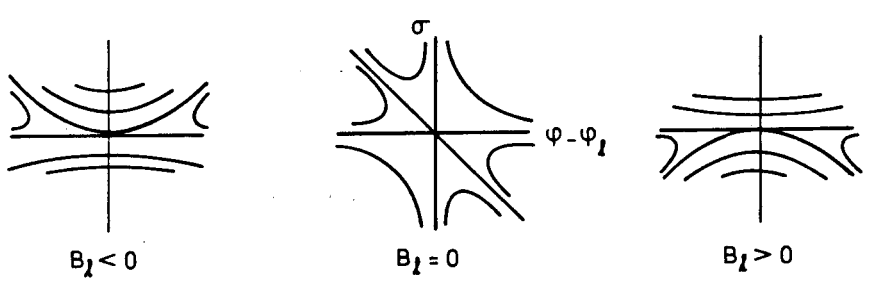

b. isobars.

FIG. 4.2 : PATTERN OF CONICAL STREAMLINES AND ISOBARS IN (φ, σ)PLANE NEAR $\varphi = \varphi_l = \frac{\pi}{2} l, l = \pm 1, \pm 3, \ldots\ldots$
$(n = 2, 2 < m < 4, \lambda = -1/2)$

from which follows that $\frac{d\varphi^*}{d\tau^*} = 0$ on the curve

$$\varphi^* = f(\sigma^*) \equiv 0 \ , \tag{4.11}$$

and that on this curve

$$\frac{d\sigma^*}{d\tau^*} = \Delta_k \, \sigma^{*k} + O(\sigma^{*k+1}) = -(m-2) \, B_\ell \, \sigma^{*2} + O(\sigma^{*3}) \ . \tag{4.12}$$

Thus, since k = 2, the equilibrium point is a saddle-node. If $B_\ell > 0$, the hyperbolic sectors contain a segment of the positive σ^* axis, if $B_\ell < 0$ a segment of the negative σ^* axis. The streamline pattern for $A_\ell = 0$ is also sketched in the (φ, σ) plane, figure 4.2a.
The possible streamline patterns near $\varphi = \varphi_\ell$, as described above, may now be used to determine the streamline patterns in the (η, ζ) plane. Obviously, only in the case m = 3 the behaviour of $F_m(\varphi)$ does not hinder the conical stagnation point to appear in a flow field away from a body surface. If higher order terms permit so, we may then derive the following streamline pattern for such a conical stagnation point. We restrict the range of φ to $0 \leq \varphi < 2\pi$, thus $\varphi_0 = 0$, $\varphi_1 = \pi/2$, $\varphi_2 = \pi$, $\varphi_3 = \frac{3\pi}{2}$. If $\varphi = \varphi_0$ (= 0) or φ_2 (= π) there is only one streamline approaching the stagnation point and for $F_0 > 0$ the streamline flows towards this point. If $\varphi = \varphi_1$ (= $\pi/2$) or φ_3 (= $3\pi/2$) there are two possibilities: there is either only one streamline approaching the stagnation point and for $F_0 > 0$ this streamline flows away from this point ($B_\ell \geq 0$), or there are an infinite number of streamlines flowing towards the stagnation point ($F_0 > 0$, $B_\ell < 0$). Since, moreover, for m = 3, $B_1 = -B_3$, there are three possibilities (i) $B_1 = 0$, $B_3 = 0$; (ii) $B_1 > 0$, $B_3 < 0$; (iii) $B_1 < 0$, $B_3 > 0$.
It may be shown that the singular points of the system (4.3) are all isolated. This means that each singular point has a neighbourhood

containing no other singular points than itself.
The argumentation given above leads to two types of streamline patterns in the (η, ζ) plane: 1) topological saddle points ($B_1 = B_3 = 0$); 2) saddle-nodes ($B_1 \neq 0$, $B_3 \neq 0$). Sketches of these flow patterns are given in figure 4.3a; with flow directions corresponding to $F_0 > 0$.

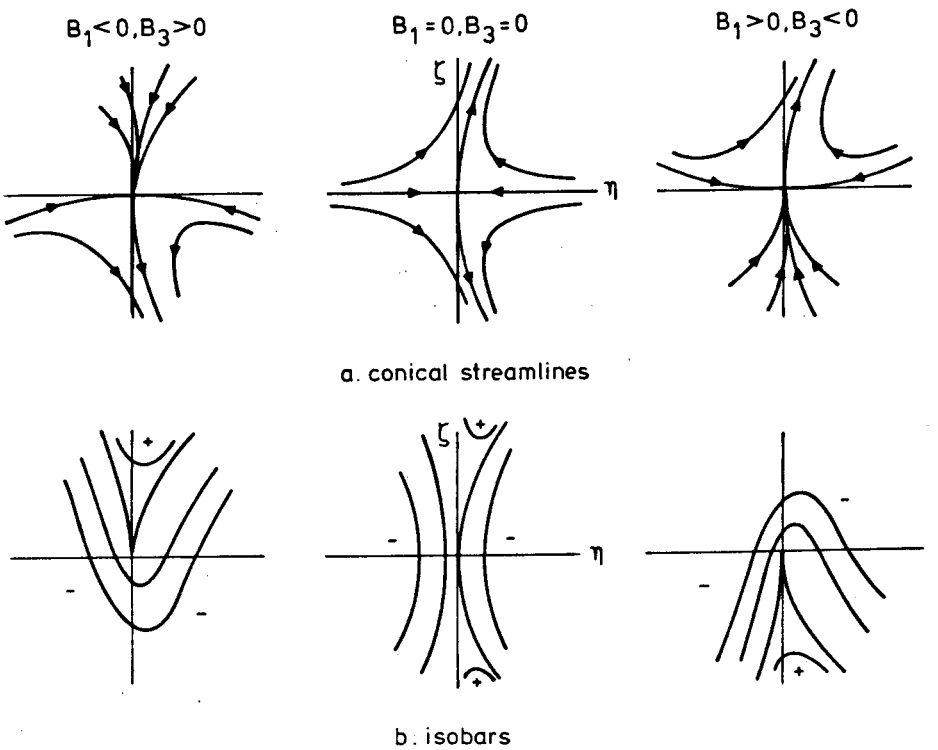

FIG. 4.3 : SADDLES AND SADDLE – NODES ($n = 2$, $m = 3$, $\lambda = -1/2$)

If $2 < m < 3$, $3 < m < 4$, equation (4.1) shows that it is not possible to fill out a full neighbourhood of the conical stagnation point with these solutions, such that the velocity is continuous. Parts of these

solutions may be used, however, to construct flows near a conical stagnation point on a body surface. It may easily be seen that the maximum sector through which such a solution can be extended is equal to $\frac{3\pi}{2}$; without loss of generality we may take $0 \leq \varphi \leq \frac{3\pi}{2}$. From figures 4.1 and 4.2 it may become apparent that four relevant combinations of B_1 and B_3 can be made: (i) $B_1 < 0$, $B_3 \gtrless 0$; (ii) $B_1 \geq 0$, $B_3 \gtrless 0$; (iii) $B_1 < 0$, $B_3 < 0$; (iv) $B_1 \geq 0$, $B_3 < 0$. The corresponding streamline patterns for $F_0 > 0$ are shown in figure 4.4a.
They may be called a partial saddle-node, a partial saddle, a partial node, and a partial saddle-node, respectively.

We now come to the determination of the isobars corresponding to the established streamline patterns. From (2.7), (4.1) the velocity components may be obtained to be

$$u = F_0 \left[1 + \tfrac{1}{2}\rho^2 \cos 2\varphi - 2\,\frac{m-1}{m}\,\mu\rho^m \cos(m\varphi + \psi_m) + o(\rho^m)\right],$$

$$v = F_0 \left[-\rho \cos\varphi + 2\mu\,\rho^{m-1} \cos\left\{(m-1)\,\varphi + \psi_m\right\} + o(\rho^{m-1})\right], \qquad (4.13)$$

$$w = F_0 \left[\rho \sin\varphi - 2\mu\,\rho^{m-1} \sin\left\{(m-1)\,\varphi + \psi_m\right\} + o(\rho^{m-1})\right],$$

and for the pressure distribution there follows

$$\left(\frac{p}{p_0}\right)^{\frac{\gamma-1}{\gamma}} = 1 - \frac{2F_0^2}{1 - F_0^2}\,G(\varphi, \rho) + o(\rho^m)\,, \qquad (4.14)$$

where $G(\varphi, \rho) = \rho^2 \cos^2\varphi - 2\mu\,\rho^m \left[2 \cos\varphi \cos\left\{(m-1)\,\varphi + \psi_m\right\} + \right.$
$\left. - \frac{1}{m} \cos(m\varphi + \psi_m)\right]$.

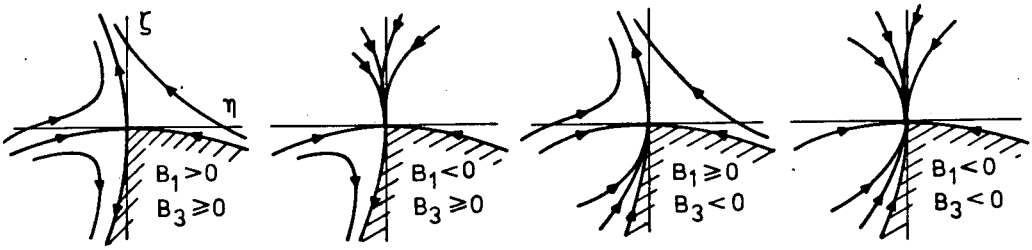

a . conical streamlines

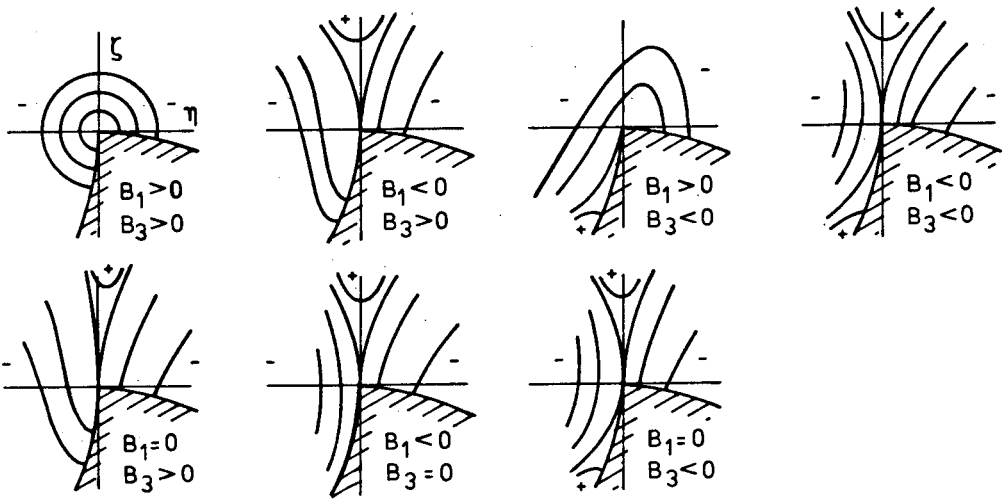

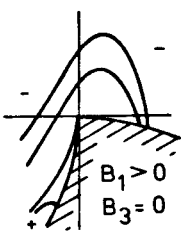

b . isobars

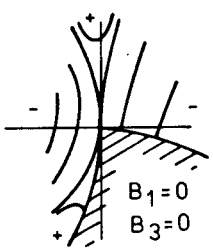

FIG . 4.4 : PARTIAL SADDLE-NODES, - TOPOLOGICAL SADDLES AND TOPOLOGICAL NODES ($n = 2, 2 < m < 3, 3 < m < 4, \lambda = -1/2$)

The isobars are, in first approximation, given by the lines G = constant, which are easier to analyse as solutions of the differential equation

$$\left(\frac{d\rho}{d\varphi}\right)_{G=\text{constant}} = -\frac{\frac{\partial G}{\partial \varphi}}{\frac{\partial G}{\partial \rho}} = \frac{\rho \sin\varphi\cos\varphi + \mu\,\rho^{m-1} f'(\varphi)}{\cos^2\varphi - \mu\, m\,\rho^{m-2} f(\varphi)}\,, \qquad (4.15)$$

where

$$f(\varphi) = 2\cos\varphi\cos\left[(m-1)\,\varphi + \psi_m\right] - \frac{1}{m}\cos\left(m\varphi + \psi_m\right)\,. \qquad (4.16)$$

Introducing a parameter τ along the isobars we may investigate (4.15) as a system in the (φ, σ) plane, where $\sigma = \rho^{m-2}$ $(\sigma \geq 0)$. Then

$$\begin{aligned} \frac{d\varphi}{d\tau} &= \cos^2\varphi - \mu\, m\,\sigma\, f(\varphi)\,, \\ \frac{d\sigma}{d\tau} &= (m-2)\,\sigma\sin\varphi\cos\varphi + \mu(m-2)\,\sigma^2 f'(\varphi)\,. \end{aligned} \qquad (4.17)$$

The singular points of this system for $\sigma = 0$ are in $\varphi = \varphi_\ell = \ell\,\frac{\pi}{2}$ $(\ell = \pm 1, \pm 3, \ldots)$. Expanding with respect to $\varphi - \varphi_\ell$ and retaining terms till the third order yields

$$\begin{aligned} \frac{d\varphi}{d\tau} &= B_\ell\,\sigma + m\,A_\ell\,\sigma\,(\varphi - \varphi_\ell) + (\varphi - \varphi_\ell)^2 - \tfrac{1}{2}m(4-3m)\,B_\ell\,\sigma(\varphi - \varphi_\ell)^2, \\ \frac{d\sigma}{d\tau} &= -(m-2)\,A_\ell\,\sigma^2 - (m-2)\,\sigma(\varphi - \varphi_\ell) + (m-2)(4-3m)\,B_\ell\,\sigma^2(\varphi - \varphi_\ell) \end{aligned} \qquad (4.18)$$

For $B_\ell \neq 0$ the eigenvalues of the linearized system are equal to zero and, similarly as before, we will follow the line of analysis given in Andronov et al. (1973), see Appendix, to investigate the integral paths of (4.18). For the curve on which $\frac{d\varphi}{d\tau} = 0$ may be found

$$\sigma = -\frac{1}{B_\ell}(\varphi - \varphi_\ell)^2 + O((\varphi - \varphi_\ell)^3) \ , \tag{4.19}$$

and on this curve there is

$$\frac{d\sigma}{d\tau} = \Delta_k (\varphi - \varphi_\ell)^k + O\left\{(\varphi - \varphi_\ell)^{k+1}\right\} = \frac{m-2}{B_\ell^2}(\varphi - \varphi_\ell)^3 + O\left\{(\varphi - \varphi_\ell)^4\right\} \tag{4.20}$$

Hence, it follows that k = 3 and Theorem II (Appendix) may be applied. As a result the equilibrium point appears to be a topological saddle point. Sketches of the isobars in the (φ, σ) plane are given in figure 4.2b.

For $B_\ell = 0$, (4.18) may be integrated to yield

$$(2A_\ell \sigma + \varphi - \varphi_\ell)\, \sigma^{\frac{2}{m-2}} (\varphi - \varphi_\ell) = C \ , \tag{4.21}$$

where C is a constant. The isobars for this case are also given in figure 4.2b. The singularity involves six hyperbolix sectors and separatrices along the φ axis, the σ axis and the line $\sigma = -A_\ell^{-1}(\varphi - \varphi_\ell)$ ($A_\ell \neq 0$, since $B_\ell = 0$ and $A_\ell^2 + B_\ell^2 \neq 0$). It should be noted that only $\sigma \geq 0$ is of interest in this investigation.

The isobar patterns in the (φ, σ) plane near $\varphi = \varphi_\ell$, as described above, may now be used to determine the isobars in the (η, ζ) plane. For m = 3 these isobar patterns are sketched in figure 4.3b, and two types are encountered: (i) a topological saddle point ($B_1 = B_3 = 0$); (ii) a degenerated saddle point ($B_1 \neq 0$, $B_3 \neq 0$). For $2 < m < 4$ ($m \neq 3$) the isobar patterns are sketched in figure 4.4b. In figures 4.3b and 4.4b regions with a pressure higher than in the stagnation point are indicated by a plus sign, whereas a lower pressure is indicated by a minus sign.

4.2. Topological saddle points, topological nodes (m = 4)

For $\lambda = \pm \frac{1}{2}$ equations (2.14), (2.16), (2.26) show that the conical potential may be written as

$$F = F_0 \left[1 \pm \tfrac{1}{2} \rho^2 \cos 2\varphi + \rho^4 \left\{ \tfrac{1}{2} \mu \cos (4\varphi + \psi_4) + \right. \right.$$

$$\left. \left. - \frac{1}{8} M_0^2 \mp \frac{1}{12} (1 - 2M_0^2) \cos 2\varphi \right\} + o(\rho^4) \right] , \qquad (4.22)$$

where $\mu = \frac{mb_m}{2F_0}$, and $M_0 = \frac{F_0}{a_0}$ is the Mach number in the conical stagnation point. We restrict ourselves to $\lambda = -\frac{1}{2}$, since the results for $\lambda = +\frac{1}{2}$ may be obtained by replacing φ by $\varphi + \frac{\pi}{2}$. Substitution of (4.22) into (2.6) leads to the equation for the streamlines

$$\frac{d\zeta}{d\eta} = \frac{-2\alpha\eta^3 - [\frac{1}{2}(1+M_0^2)+6\beta]\eta^2\zeta + 6\alpha\eta\zeta^2 + [\frac{1}{6}(1+M_0^2)+2\beta]\zeta^3 + o((\eta^2+\zeta^2)^{3/2})}{-2\eta - [\frac{1}{6}(1+7M_0^2)-2\beta]\eta^3 - 6\alpha\eta^2\zeta + [\frac{1}{2}(1-M_0^2)-6\beta]\eta\zeta^2 + 2\alpha\zeta^3 + o((\eta^2+\zeta^2)^{3/2})} , \qquad (4.23)$$

where $\alpha = \mu \sin \psi_4$, $\beta = \mu \cos \psi_4$. The point $\eta = \zeta = 0$ is a multiple equilibrium point, which may be analyzed similarly as in previous cases. Applying Theorem I of the Appendix we find that the point is a topological node for $\beta < -\frac{1}{12}(1 + M_0^2)$ and a topological saddle point for $\beta > -\frac{1}{12}(1 + M_0^2)$. For $\beta = -\frac{1}{12}(1 + M_0^2)$ and $\alpha \neq 0$, also a topoligical saddle point occurs. The case $\beta = -\frac{1}{12}(1 + M_0^2)$ and $\alpha = 0$ cannot be considered without taking into account higher order terms in the expansion for F.

The isobars are the integral paths of the differential equation

$$\frac{d\zeta}{d\eta} = \frac{\eta + \left(-7\beta + \frac{11}{12} - \frac{49}{12} M_0^2\right)\eta^3 + 15\alpha\eta^2\zeta - \left(-9\beta + \frac{1}{4} - \frac{3}{4} M_0^2\right)\eta\zeta^2 - \alpha\zeta^3 + o((\eta^2+\zeta^2)^{3/2})}{-5\alpha\eta^3 + \left(-9\beta + \frac{1}{4} - \frac{3}{4} M_0^2\right)\eta^2\zeta + 3\alpha\eta\zeta^2 - \left(\beta + \frac{1}{12} M_0^2 + \frac{1}{12}\right)\zeta^3 + o((\eta^2+\zeta^2)^{3/2})} \qquad (4.24)$$

Following again the Appendix Theorem II yields that for $\beta < -\frac{1}{12}(1 + M_0^2)$ and for $\beta = -\frac{1}{12}(1 + M_0^2)$ but $\alpha \neq 0$ the isobars form a topological saddle point whereas for $\beta > -\frac{1}{12}(1 + M_0^2)$ a centrepoint singularity occurs. Streamline patterns for $F_0 > 0$ and isobars are sketched in figure 4.5.

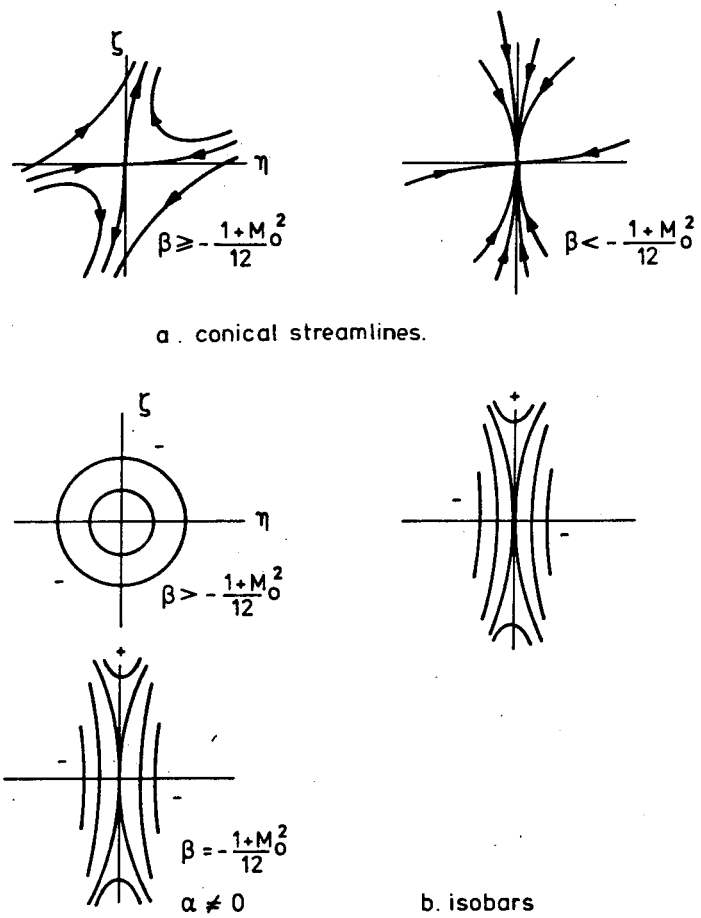

FIG. 4.5 : TOPOLOGICAL SADDLES AND NODES.
(n = 2 , m = 4 , λ = -½)

4.3. Discussion of results

The higher order singularities, only occurring for n = 2 and $|\lambda| = \frac{1}{2}$, discussed in the preceding sections of this paragraph are structurally unstable. The singularities consist of saddle-nodes, topological saddles and topological nodes. The structural instability will manifest itself in such a way that small changes in a flow parameter cause bifurcation, as a result of which the topological character of the streamline pattern changes (Andronov et al. 1971).

For example, the lift-off phenomenon of the singularity occurring in the supersonic flow field past a circular cone at high incidences leads the attention to these singularities. The lift-off phenomenon may then be viewed as a bifurcation phenomenon. At the lift-off angle of incidence the body conical stagnation point in the leeward symmetry plane would be a saddle-node. The nodal part would be formed by the streamlines outside of the body surface. The saddle part would be found if the flow around the body would be extended inside the body. Increasing the angle of incidence beyond the lift-off angle makes the saddle-node fall apart into a saddle point attached to the cone surface and a nodal point moving away from the body surface. Decreasing the angle of incidence below the lift-off angle would leave a nodal point on the cone surface and create a saddle point moving into the solution inside the cone. The calculations made by Bakker & Bannink (1974) to investigate conical stagnation points within the framework of slender body theory may be used to support the bifurcation point of view of the lift-off phenomenon. In experiments viscosity tends to obscure the lift-off phenomenon, which starts at a point of the body surface, so that the boundary layer is dominant. This may be observed i.e. in the experiments reported by Bannink & Nebbeling (1978) and Nebbeling & Bannink (1978). In these experiments the flow field past a cone with 7.5^{o} semi-apex angle was investigated at angles of incidence from 17^{o} to 22^{o} in a supersonic flow with a Mach number of 2.94. It was observed that, at high incidences, flow separation leads to the generation of a vortex system at the leeward side of the cone. The appearance of a dividing streamline, separating

the vortex system from the remainder of the flow field, may be explained in terms of another bifurcation occurring in the flow field. A known bifurcation of a saddle-node is its falling apart into either a saddle and a node or its disappearance leaving no singularity at all. The occurrence of the dividing streamline and the related saddle point in the leeward symmetry plane, accompanied by a nodal conical stagnation point higher above the cone surface may then be understood as a bifurcation from a saddle-node singularity appearing in the flow field at some angle of incidence between 17^{o} and 22^{o}.

5. CONCLUSIONS

The main results obtained in this report are summarized in the following:

- Solutions of the Laplace equation, describing the incompressible plane flow between two intersecting walls are useful as a guide to generate solutions near conical stagnation points in a potential conical flow.
- Conical stagnation point solutions may be subdivided into first order structurally stable and higher order structurally unstable solutions.
- In the class of first order singularities, conical streamline patterns such as nodes and saddles, already known in the literature, are found. In addition an oblique saddle point flow pattern is found inside a corner with an including angle between $\frac{\pi}{2}$ and π rad. The first order singularities are shown in figures 3.1, 3.2 and 3.4.
- The oblique saddle point solution may be used to describe the inviscid flow pattern associated with flow separation and it may also explain certain features of the supersonic flow past an external corner.
- Although the incompressible plane flow solutions suggest the existence of conical saddle point flow in a corner with an including angle less than $\frac{\pi}{2}$ rad, the latter type of flow could not be established within the framework of conical potential flow theory.
- The class of higher order singularities consists of saddle-nodes, topological saddles and topological nodes. These singularities are structurally unstable in the sense that a slight deviation of a flow parameter causes a bifurcation, as a result of which the topological character of the singularity may change.
  The higher order singularities are given in figures 4.3, 4.4 and 4.5.
- The lift-off phenomenon of the singularity in the supersonic flow past a circular cone at incidence may be interpreted as a bifurcation of a saddle-node into a saddle and a node. Similarly, this may be done for the appearance of the dividing streamline in the same flow at still higher angles of incidence, such that a vortex system is formed at the leeward side of the cone.

6. REFERENCES

Andronov, A.A., Leontovich, E.A., Gordon, J.J. & Maier, A.G. 1971. Theory of bifurcations of dynamic systems on a plane. John Wiley & Sons, New York, Toronto.

Andronov, A.A., Leontovich, E.A., Gordon, J.J. & Maier, A.G. 1973. Qualitative theory of second-order dynamic systems. John Wiley & Sons, New York, Toronto.

Bakker, P.G. 1977. Conical streamlines and pressure distribution in the vicinity of conical stagnation points in isentropic flow. Report LR-244, Delft University of Technology, Department of Aerospace Engineering.

Bakker, P.G. & Bannink, W.J. 1974. Conical stagnation points in the supersonic flow around slender circular cones at incidence. Report VTH-184, Delft University of Technology, Department of Aerospace Engineering.

Bannink, W.J. & Nebbeling, C. 1978. Measurements of the supersonic flow field past a slender cone at high angles of attack. AGARD-CP-247, Paper 22.

Coddington, E.A. & Levinson, N. 1955. Theory of ordinary differential equations. McGraw-Hill, New-York.

Ferri, A. 1951. Supersonic flow around circular cones at angles of attack. NACA TR 1045.

Fletcher, C.A.J. 1975. GTT method applied to cones at large angles of attack. Proc. 4th Int. Conf. Num. Meth. Fluid Dyn., Ed. R. Richtmyer, Lecture Notes in Physics, Vol. 35, Springer Verlag, West-Berlin.

Kutler, P. & Shankar, V. 1976. Computation of the inviscid supersonic flow over an external axial corner. Proc. 1976 Heat Transfer & Fluid Mech. Inst., Davis, Calif., p. 356-373.

McRae, D.C. & Hussaini, M.Y. 1978. Numerical simulation of supersonic cone flow at high angle of attack. AGARD-CP-247, Paper 23.

Melnik, R.E. 1967. Vortical singularities in conical flow. AIAA Journal, Vol. 5, No. 4, p. 631-637.

Nebbeling, C. & Bannink, W.J. 1978. Experimental investigation of the supersonic flow past a slender cone at high incidence. Journal of Fluid Mechanics. Vol. 87, part 3, p. 475-496.

Salas, M. & Daywitt, J. 1978. Structure of the flow field about external axial corners. AIAA Paper 78-59.

Smith, J.H.B. 1972. Remarks on the structure of conical flow. Progress in Aerospace Sciences, Vol. 12, Pergamon Press, London, p. 241-272.

APPENDIX

TOPOLOGICAL STRUCTURE OF A MULTIPLE EQUILIBRIUM STATE

Consider the system

$$\frac{dx}{dt} = P(x,y) \ , \quad \frac{dy}{dt} = Q(x,y) \tag{A.1}$$

where $P(x,y)$ and $Q(x,y)$ are analytic functions.
Let $O(0,0)$ be an isolated equilibrium state of this system at the origin, so that there exists a neighbourhood of O containing no other equilibrium states than O, and let $P(0,0) = Q(0,0) = 0$.
Suppose that the Taylor expansion of the functions $P(x,y)$ and $Q(x,y)$ about the equilibrium state $O(0,0)$ have the form

$$\frac{dx}{dt} - ax + by + P_2(x,y) \ , \quad \frac{dy}{dt} = cx + dy + Q_2(x,y) \tag{A.2}$$

where $P_2(x,y)$ and $Q_2(x,y)$ are analytic in the neighbourhood of the origin and their series expansion involve only terms of at least second order.

If the determinant of the coefficient matrix of the linearized system $\Delta = \begin{vmatrix} a & b \\ c & d \end{vmatrix} = 0$ the structure of the equilibrium state may not be identical with that of the linearized system and a multiple equilibrium state is present.

The following discussion on multiple equilibrium states is restricted to systems where the expansion of the right hand sides in the neighbourhood of $O(0,0)$ involves at least one first order term.
If $\Delta = 0$ one or both eigenvalues of the coefficient matrix $\begin{pmatrix} a & b \\ c & d \end{pmatrix}$ are zero. In the next both cases will be considered separately.

Multiple equilibrium state with one zero eigenvalue

Consider system (A2) with the assumptions

$$\Delta = ad - bc = 0 \ , \quad \Sigma = a + d \neq 0$$

Under these assumptions there exists a non singular transformation which reduces system (A.2) into the form

$$\frac{dx}{dt} = P_2(x,y) = P(x,y) \ , \quad \frac{dy}{dt} = y + Q_2(x,y) = Q(x,y) \tag{A.3}$$

Let $\Sigma(x,y) = \frac{\partial P}{\partial x} + \frac{\partial Q}{\partial y}$ where $P(x,y)$ and $Q(x,y)$ are functions given in (A.3).

The function $\Sigma(x,y)$ is continuous with $\Sigma(0,0) = 1$.

Because $O(0,0)$ is an isolated equilibrium state there exists a sufficiently small neighbourhood $U_\delta(O)$ of 0 where $\Sigma(x,y) > 0$. This implies that $U_\delta(O)$ contains neither closed paths nor loops. Hence there must exist integral curves that tend to the equilibrium point. These integral curves are called semi paths of the system which tend to $O(0,0)$ is a definite direction θ^* where

$$\frac{dy}{dx} = \frac{y}{x} = \tan \theta^* \tag{A.4}$$

For the system (A.3) the directions in which semi paths tend to $O(0,0)$ are then 0, $\frac{\pi}{2}$, π and $\frac{3\pi}{2}$ rad.

To obtain the possible topological structures of the equilibrium state consider the equation

$$y + Q_2(x,y) = 0 \tag{A.5}$$

This equation has a solution $y = \varphi(x)$ in a small neighbourhood of $O(0,0)$ such that $\varphi(0) = 0$, $\varphi'(0) = 0$. The curve $y = \varphi(x)$ is an isocline of horizontal directions $\left(\frac{dy}{dt} = 0\right)$.

Define a function

$$\psi(x) = P_2(x, \varphi(x)) \tag{A.6}$$

which describes the value of $\frac{dx}{dt}$ on the curve $\frac{dy}{dt} = 0$.

Because $O(0,0)$ is isolated, $\psi(x)$ cannot vanish identically and the series expansion of $\psi(x)$ assumes the form

$$\psi(x) = \Delta_k x^k + \ldots\ldots \tag{A.7}$$

where $k \geq 2$, $\Delta_k \neq 0$.

The possible topological structure of an equilibrium state $O(0,0)$ of the system (A.3) is established by the following theorem.

Theorem I

Let $O(0,0)$ be an isolated equilibrium state of the system (A.3). Let $y = \varphi(x)$ be an solution of the equation $y + Q_2(x,y) = 0$ in the neighbourhood of $O(0,0)$, and assume that the series expansion of the function $\psi(x) = P_2(x, \varphi(x))$ has the form $\psi(x) = \Delta_k x^k + \ldots\ldots$, where $k \geq 2$, $\Delta_k \neq 0$. Then:

1. If k is odd and $\Delta_k > 0$, $O(0,0)$ is a topological node (figure A.1).
2. If k is odd and $\Delta_k < 0$, $O(0,0)$ is a topological saddle point (figure A.2), two of whose separatrices tend to O in the directions 0 and π, the other two in the directions $\pi/2$ and $3\pi/2$.
3. If k is even, $O(0,0)$ is a saddle-node, i.e. an equilibrium state whose neighbourhood is the union of one parabolic and two hyperbolic sectors. If $\Delta_k < 0$ the hyperbolic sectors contain a segment of the positive x-axis (figure A.3); if $\Delta_k > 0$ they contain a segment of the negative x-axis.

The proof of this theorem is given in Andronov et al. 1973, pp. 340-346.

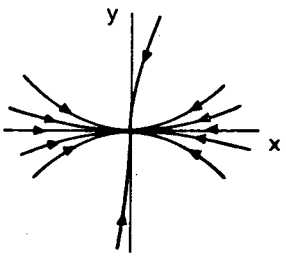

FIG. A1

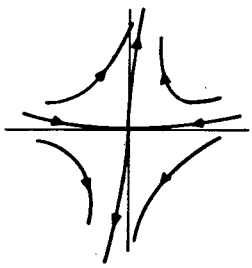

FIG. A2

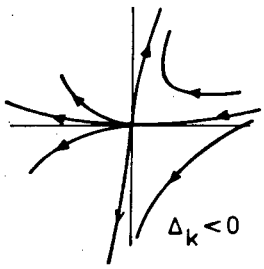

FIG. A3

Multiple equilibrium state with zero eigenvalues

Now the system (A.2) is considered with the assumptions

$$\Delta = ad - bc = 0 \ , \quad \Sigma = a + d = 0 \ , \quad |a| + |b| + |c| + |d| \neq 0$$

There exists a non-singular transformation which reduces the system (A.2) to

$$\frac{dx}{dt} = y + P_2(x,y) \ , \quad \frac{dy}{dt} = Q_2(x,y) \tag{A.8}$$

where $P_2(x,y)$ and $Q_2(x,y)$ are analytic in the neighbourhood of $O(0,0)$ and their series expansion involve only terms of at least second order. The topological structure of the equilibrium state $O(0,0)$ of this system follows by considering the solution $y = \varphi(x)$ of the equation

$$y + P_2(x,y) = 0 \tag{A.9}$$

The curve $y = \varphi(x)$ is an isocline if vertical directions $\left(\frac{dx}{dt} = 0\right)$.

On this curve the functions

$$\psi(x) = Q_2(x, \varphi(x)) \text{ and } \Sigma(x) = \frac{\partial P_2}{\partial x}(x, \varphi(x)) + \frac{\partial Q_2}{\partial y}(x, \varphi(x))$$

may be expanded as follows

$$\psi(x) = \Delta_k x^k + \ldots\ldots , \quad \Sigma(x) = b_n x^n + \ldots\ldots$$

where Δ_k and b_n are the first non vanishing coefficients $\psi(x)$ and $\Sigma(x)$, respectively. If $\Sigma(x) \equiv 0$, then $b_n = 0$. The topological structure of an equilibrium state of the system (A.8) is established by the following theorem.

Theorem II

- Let the number k be odd, $k = 2m + 1$ $(m \geq 1)$, and $\lambda = b_n^2 + 4(m+1)\Delta_k$. Then if $\Delta_k > 0$, the equilibrium state of system (A.8) is a topological saddle point (figure A.4). But if $\Delta_k < 0$, the point O is
  1. a focus or center if $b_n = 0$, or if $b_n \neq 0$ and $n > m$, or if $b_n \neq 0$, $n = m$ and $\lambda < 0$ (figures A.5, A.6);
  2. a topological node if $b_n \neq 0$, n is even and $n < m$, or if $b_n \neq 0$, n is even, $n = m$ and $\lambda \geq 0$ (figure A.1);
  3. an equilibrium state with an elliptic region if $b_n \neq 0$, n is odd and $n < m$, or if $b_n \neq 0$, n is odd, $n = m$ and $\lambda \geq 0$ (figure A.7).

- Let the number k be even, $k = 2m$ $(m \geq 1)$.
  Then the equilibrium state $O(0,0)$ is
  1. a degenerate equilibrium state if $b_n = 0$, or $b_n \neq 0$ and $n \geq m$ (figure A.8);
  2. a saddle-node if $b_n \neq 0$ and $n < m$ (figure A.9).

The proof of this theorem is given in Andronov et al. 1973 (pp. 357-363).

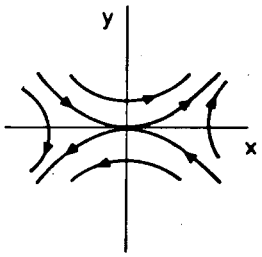

FIG. A4

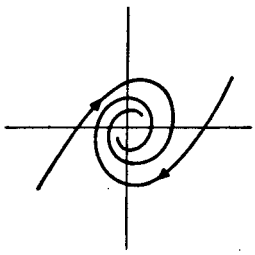

FIG. A5

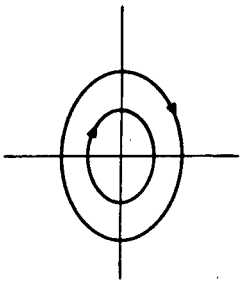

FIG. A6

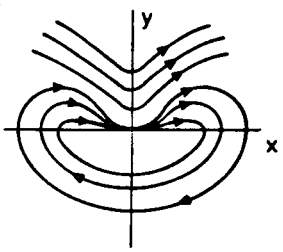

FIG. A7

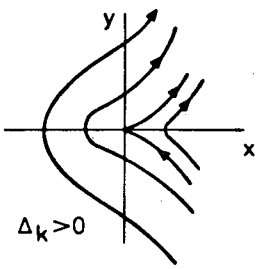

FIG. A8

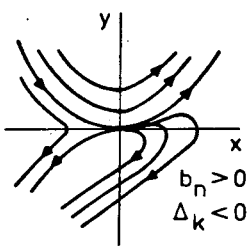

FIG. A9